# DYNAMIC BIAXIAL STRESS ANALYSIS OF FLAT LAYERED CERAMIC COMPOSITES

## ANALIZA DVOOSNIH DINAMIČNIH NAPETOSTI V RAVNIH PLASTOVITIH KERAMIČNIH KOMPOZITIH

**Milan Ambrožič[1,2]\*, Anatolij Nikonov[2]**

[1]Faculty of Mathematics and Natural Sciences, University of Maribor, Koroška 160, 2000 Maribor, Slovenia
[2]Faculty of Industrial Engineering, Šegova 112, 8000 Novo mesto, Slovenia

We study theoretically the biaxial bending of symmetric, flat layered ceramic composites (laminates) due to external loading. We focus on three-layered alumina/zirconia laminates. We compare the principal stresses in the samples in the case of static and harmonic dynamic loading. The dynamic equation within the Kirchhoff theory for thin homogeneous plates is first generalized to the case of multilayered plates. It is solved numerically with the relaxation method, which we have developed for this purpose.

Keywords: layered ceramic composites, Kirchhoff theory of plates, biaxial stress, principal stresses

Teoretično smo študirali dvoosni upogib simetričnih ravnih plastovitih keramičnih kompozitov (laminatov) zaradi zunanje obremenitve. Osredotočili smo se na triplastne laminate iz aluminijevega in cirkonijevega oksida. Primerjali smo lastne vrednosti napetosti za statično in harmonično dinamično obremenitev. Dinamično enačbo v okviru Kirchhoffove teorije za homogene tanke plošče smo najprej generalizirali za primer večplastnih plošč. Enačbo smo reševali numerično z relaksacijsko metodo, ki smo jo razvili v ta namen.

Ključne besede: plastoviti keramični kompoziti; Kirchhoffova teorija plošč; dvoosna napetost; lastne vrednosti napetosti

## 1 INTRODUCTION

Alumina ($Al_2O_3$) based ceramics are frequently used in various applications, such as cutting tools and biomedical implants, because of their good mechanical properties. Pure alumina has high hardness and low weight, but a relative moderate bend strength and fracture toughness. Zirconia ($ZrO_2$) can have significantly higher fracture toughness and bend strength than alumina. Therefore, composites of alumina with an appropriate volume fraction of tetragonal zirconia (zirconia toughened alumina, ZTA) are promising materials due to a high bend strength and fracture toughness, as well as wear resistance.[1–6] F. Sommer et al.[6] have reported that using 1 mol. % of yttria can raise the bend strength of ZTA ceramics (containing 17 vol. % of yttria stabilized zirconia) up to nearly 1200 MPa and the ISB fracture toughness up to 8.5 MPa $\sqrt{m}$.[6] Multi-layered alumina/zirconia composites (laminates) have been studied particularly in regard to residual and loading stresses.[7–12] Thermal residual stresses within individual layers arise upon cooling the material after the sintering process because of the mismatch of the thermal expansion coefficients of alumina and zirconia.

Various static uniaxial or biaxial bending tests are used to measure the strength of ceramic samples. E. Carrera and A. Ciuffreda[13] compared a three-dimensional stress distribution in composite plates from different theories and validated their results for different static loadings with the finite-element method (FEM). However, the ceramic and other engineering products/components are often subjected to dynamic loads in everyday use. Therefore, different aspects of the dynamics of elastic plates, shells and beams have been investigated thoroughly. A particular interest has been devoted to the propagation of traction-free elastic waves in thin flat plates, theoretically with a finite thickness but infinite lateral dimensions. An analytical approach shows that even for homogeneous and symmetric three-layered plates the ordinary equations for dispersion relations and the corresponding strains and stresses are complex.[14–16] Different analytical or semi-analytical approaches for finite plates can be used only when the problem is effectively one-dimensional (1D) and the boundary conditions are simple. Z. J. Ai et al.[17] studied the problem of an elastic plate on the stack of layers with the uniformly moving load on the plate, where they used the Fourier transformation and analytical layer method. An interesting idea for the partially analytical approach for the two-dimensional (2D) problem of multilayered plate dynamics was given by M. Sharyjat and M. Roshanfar.[18] They expanded the deflection of the plate with sine functions of coordinates and with time-dependent coefficients.

---

\*Corresponding author's e-mail:
milan.ambrozic@um.si (Milan Ambrožič)

Numerical calculations for the biaxial deformations of finite plates include several variants of FEM methods. Zhang et al. have developed an efficient two-step FEM method for the calculation of the dynamics and stresses in multilayered plates: the method is composed of a fine-scale computation for parts of the system, followed by a coarse-scale computation for the whole system.[19] Among various numerical methods for the three-dimensional (3D) problem of multilayered plates we mention a very sophisticated sampling surface method, where the basic variables are a dense set of inner sampling surfaces. T. Ye et al.[20] implemented this method with the spectral expansion technique where the basic orthogonal functions are Chebyshev polynomials. Using this approach, they were able to reach a highly accurate numerical precision, even for relatively thick plates with various boundary conditions. There are several other approaches and techniques to attack the problem of multilayered plates, but they are not focused directly on the simple single equation for the dynamic bending of the plate as a whole.[21–24] As regards the parabolic-type fourth-order classic equation for bending deformation of thin plates within the Kirchhoff theory, several attempts have been made to refine the theory, particularly for infinite plates, including Timoshenko-Reissner-Mindlin type theories.[25]

In this paper we use the simple Kirchhoff theory for pure 2D bending deformation and generalize the dynamic equation of a homogeneous plate to the case of multilayered plates. The dynamic equation is solved numerically on a discrete network with a relaxation method. We are particularly interested how the frequency of the external load and the composition of the sample influence the stress magnitude in the 3-layered alumina/zirconia sample. A benefit of our approach is that we present the vibration of the plate as a single object. The parameters of different layers enter a single dynamic equation only through the composed flexural rigidity, without the necessity of solving the coupled system of equations for different layers simultaneously. After the dynamic equation is solved, the stress tensor is calculated in each layer separately. It may be interesting from the mathematical point, that the efficiency of the relaxation method for the fourth-order equation is not significantly different from that for elliptic-type equations of the second order.

## 2 NUMERICAL MODEL

Let us first consider the case of a homogeneous, thin square plate subject to bending deformation. Its Young's modulus, Poisson's ratio and mass density are $E$, $\nu$ and $\rho$, respectively. The thickness of the plate is $h$, while its side is $2a$. We choose the Cartesian coordinate system with the origin at the center of the plate, the $z$–axis is perpendicular to the plate, and the other two axes parallel to the

sides of the plate. The neutral plane is at $z = 0$. The deformation according to the Kirchhoff theory for a thin plate is characterized by the displacement $w(x, y, t)$ of the points on the neutral plane in the direction of $z$–axis. The corresponding dynamic equation for the "displacement function" $w$ is:

$$D(\nabla^2)^2 w + \rho h \frac{\partial^2 w}{\partial t^2} = p \tag{1}$$

where $\nabla^2 = \partial^2/\partial x^2 + \partial^2/\partial y^2$ is the 2D Laplacian.[26,27] The quantity $p$ on the right side of Equation (1) is the external pressure difference on both sides of the plate. In general, it can be a function of $x$, $y$ and $t$. The flexural rigidity (bending stiffness) for a homogeneous plate is:

$$D = \frac{Eh^3}{12(1-\nu^2)} \tag{2}$$

A convenient numerical form of Equation (1) and its extension to a layered plate in dimensionless units (denoted by $*$) are given in *Appendix A*. We take some reference Young's modulus $E_0$ and density $\rho_0$, so that $E^* = E/E_0$, $p^* = p/E_0$ and $\rho^* = \rho/\rho_0$. We introduce the reference flexural rigidity as $D_0 = E_0 h^3$ instead of Equation (2), and the dimensionless flexural rigidity is $D^* = D/D_0$.

The coordinates and displacement are normalized as: $x^* = x/a$, $y^* = y/a$, $z^* = z/h$ and $w^* = w/h$. We define the ratio $\eta = h/a$, which is supposed to be small. A suitable choice for the dimensionless time is $t^* = t/t_0$, where the characteristic time is:

$$t_0 = \sqrt{\frac{\rho_0}{E_0}} \cdot \frac{a^2}{h} = \sqrt{\frac{\rho_0}{E_0}} \cdot \frac{a}{\eta} \tag{3}$$

This expression gives a correct order of magnitude of the lowest eigenfrequency $\nu = 1/t_0$. When the function $w^*$ is found, the components of the strain and stress tensors can be calculated; see the explanation in the textbook of by Landau and Lifshitz[26] and additional details in the papers of V. V. Vasiliev[27] and N. I. Robinson.[28] The basic assumption in the derivation of equations for thin plates is that the stress components $\sigma_{xz}$, $\sigma_{yz}$ and $\sigma_{zz}$ can be neglected in comparison with $\sigma_{xx}$, $\sigma_{yy}$ and $\sigma_{xy}$. The eigenvalues $\sigma_1$ and $\sigma_2$ (principal stresses) of the remaining 2D stress tensor can finally be calculated. The direct relationship between the stress tensor and the displacement function $w^*$ is given in Appendix A.

We present in this paper the results for homogeneous pressure over the plate. For static loading the constant pressure $p^*_0$ is applied. In the case of harmonic dynamic loading we take: $p^* = p^*_0 \sin(2\pi\nu_{app}t)$, with applied frequency $\nu_{app}$ and the corresponding period $T_{app} = 1/\nu_{app}$. We present the results for clamped edges (rigid boundary with zero values of displacement and its normal derivative): (I) $w = 0$ and $\partial w/\partial x = 0$ for $x = \pm a$; (II) $w = 0$ and $\partial w/\partial y = 0$ for $y = \pm a$.

# 3 RESULTS AND DISCUSSION

## 3.1 Analysis of a homogeneous plate

Typical symmetrically positioned representative points of the plate at $z = 0$ are indicated in **Figure 1**.

First, we consider a homogeneous "plate". We choose a homogeneous alumina sample with the following parameters (**Table 1**): $2a = 100$ mm, $h = 5$ mm ($\eta = 0.1$), $E = E_0 = 390$ GPa, $\nu = 0.238$, $\rho = \rho_0 = 3.98$ kg/dm$^3$, $p_0 = 1$ MPa. The time dependence of the displacement of three representative points in the harmonic loading is compared in **Figure 2**, where we choose $T_{app}^* = 10$.

The period of the basic eigenmode is estimated: $T^* = 2.32$ or $T_A = T^* t_0 = 117$ $\mu$s (Equation (3)); the corresponding eigenfrequency is $\nu_A = 1/T_A = 8.53$ kHz (the index "A" stands for alumina).

To represent the distribution of stress we take a static loading with pressure $p_0 = 1$ MPa. **Figure 3** shows the profile of both principal stresses along two symmetry
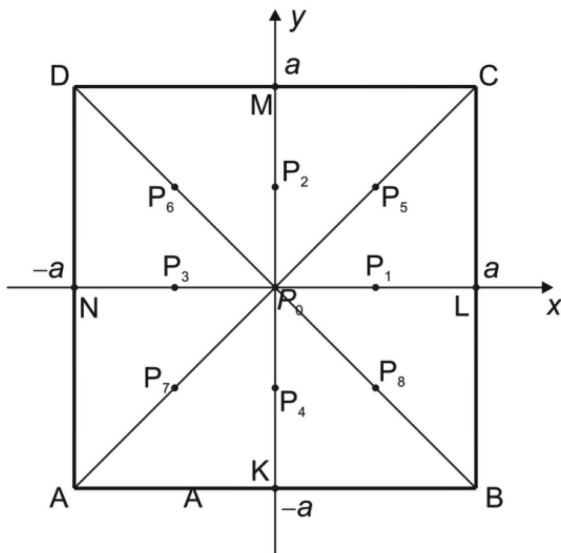
lines: $y = 0$ (horizontal line through points N, P$_3$, P$_0$, P$_1$ and L); 2) and $y = x$ (diagonal line through points A, P$_7$, P$_0$, P$_5$ and C). The principal stresses $\sigma_1$ and $\sigma_2$ at the central point P$_0$ are equal due to symmetry ($x^* = 0$ in **Figure 3**).

The lines on the top plate's surface are taken ($z = h/2$) in **Figure 3**. We are interested in positive (tensile) stresses, which are much more detrimental for ceramic materials than compressive stresses. However, the strongly negative value $\sigma_2 \approx -120$ MPa at the edges means that the corresponding principal stress is +120 MPa on the opposite surface ($z = -h/2$), at the point with the same coordinates $x^*$ and $y^*$. The largest stresses thus correspond to edge points K, L, M and N in **Figure 1**, not to the central point P$_0$. The static displacement of P$_0$ is $w^*_{stat} = w^*(0, 0) = 0.0057$, or $\approx 0.03$ mm in physical units.

## 3.2 Analysis of 3-layered plate

Now, we focus on the ZTA composites and we keep the same dimensions as given above. We take a symmetric 3-layered composite with alumina outer layers and a ZTA inner layer. The corresponding material parameters, presented in **Table 1**, can be obtained from several references.[10,11] Only the value 500 MPa for the strength of pure alumina has been chosen rather arbitrarily. This is, because the data from literature vary significantly due to different fabrication procedures.[1,10,11]

**Table 1:** Material parameters of pure alumina (A) and a particular ZTA composite: Young's modulus, Poisson's number, density and approximate bend strength

| Material | $E$ (GPa) | $\nu$ | $\rho$ (g/cm$^3$) | $\sigma_b$ (MPa) |
|----------|-----------|-------|-------------------|------------------|
| A | 390 | 0.238 | 3.98 | 500 |
| ZTA24 | 338 | 0.264 | 4.48 | 850 |



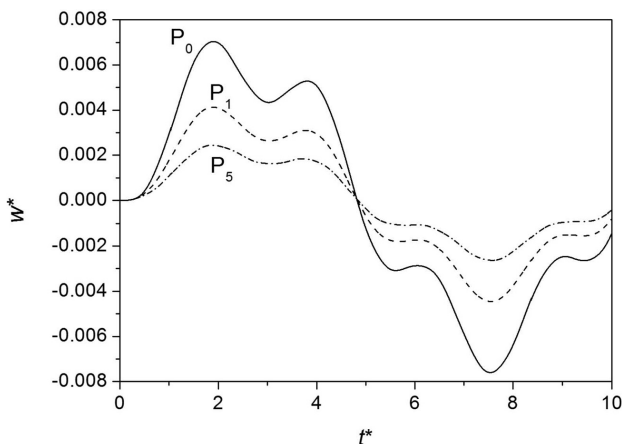**Figure 1:** Location of representative points on the square plate



**Figure 2:** Time-dependent displacements of the plate at points P$_0$ (solid line), P$_1$ (dashed line) and P$_5$ (dash–dotted line) located at $z = 0$ plane for harmonic pressure variation; $T_{app}^* = T_{app}/t_0 = 10$
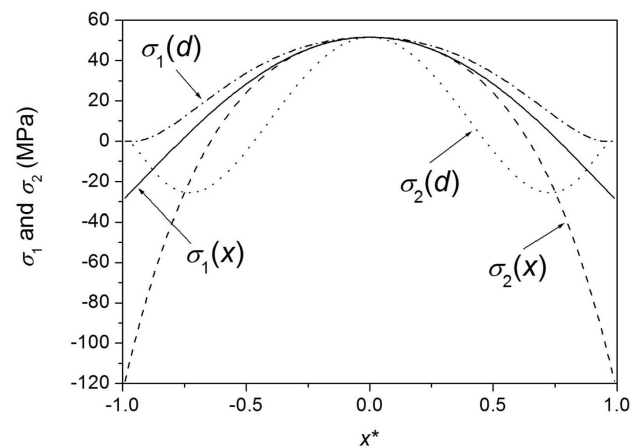


**Figure 3:** Line profile of both principal stresses: dependence on $x^* = x/a$. Here, $\sigma_1 > \sigma_2$ is chosen, regardless of the corresponding eigenvectors. The symbol ($x$) attached to graphs denotes the $y = 0$ line, and the symbol ($d$) the $y = x$ diagonal line. Solid and dashed curves: $\sigma_1$ and $\sigma_2$ on $y = 0$ line, respectively; dash-dotted and dotted lines: $\sigma_1$ and $\sigma_2$ on $y = x$ line, respectively

We have varied systematically the thickness of the middle layer (keeping the total thickness as 5 mm) as well as the frequency of the pressure oscillation. Besides the pure alumina plate, we choose a ZTA24 composite (with 24 % of mass fractions of yttria stabilized zirconia) for the middle layer.[6] The lowest eigenfrequency $\nu_A = 8.53$ kHz for the alumina sample is the basis for the set of testing applied frequencies for all the samples. The maximum value of the larger value of the pair $(\sigma_1, \sigma_2)$ over testing time and over the whole sample is traced. We call this "maximum stress" for briefness and denote it with $\sigma_{max}$. The simulation time is several periods $T_{app}$. The graphs for three compositions are presented in **Figure 4**. It has been verified in all cases that the maximum stress appears at the edge points K, L, M and N in **Figure 1**, both for static and dynamic pressure. The maximum stress at the point $P_0$ is roughly twice smaller. The maximum stress increases steadily with the frequency $\nu_{app}$. It also slightly increases with the thickness of the ZTA middle layer. The exception is the largest frequency $\nu_{app} = \nu_A$, where the maximum stress of pure alumina is the largest. This is easily explained, since the calculations show that when the thickness of the ZTA middle layer increases, the corresponding period $T^*$ for the first eigenmode increases from 2.32 for alumina to 2.61 for composite with 4.8 mm ZTA inner layer. Thus, for $\nu_{app} = \nu_A$ the two comparable ZTA composites are slightly out of their own eigenfrequencies.

Finally, we should stress another point. No damping of the plate oscillation has been considered in the presented results for two reasons: (1) because of the lack of corresponding data for ceramics, (2) because the inclusion of the contribution of the individual layers to total damping is not straightforward. We have nevertheless tried to make a simple modification of the dynamic equation in order to get some insight how the damping could influence the stresses in the material. Damping can be introduced by an additional term $\beta^* \partial w^*/\partial t^*$ on the left side of the dimensionless Equation (A.1). The dimensionless parameter $\beta^*$ represents the strength of damping, and the two terms with time derivatives on the left side of the upgraded equations compete. To test the case of moderate damping, we have chosen a particular value $\beta^* = \rho^*/10$, just for the pure alumina sample. As expected, the maximum stress in the sample is decreased when the damping is present. For frequency $\nu_{app} = \nu_A/8$, the maximum stress is 2 % lower than without damping. Even at $\nu_{app} = \nu_A/2$ the difference in maximum stress is only 4 %, while for $\nu_{app} = \nu_A$ this difference becomes more significant: 20 %. We note that our criterion for the maximum stress is not the steady state, when the vibration eigenmodes cease, but we have checked the stresses from the beginning of vibration. The stresses in the steady state instead of the transient part of vibration can be simply traced, after many periods $T_{app}$ are elapsed.

## 4 CONCLUSIONS

We have found that by increasing the frequency of the applied harmonic pressure from zero (static load) up to the "resonant" frequency the stresses in the ceramic composite laminate are increased by an order of magnitude. For the frequencies about 1/8 of eigenfrequency, i.e., of the order kHz in our case, the dynamic stresses in the composite differ from the corresponding static values only by 10 %. Furthermore, while for static loading the differences in maximum stresses are relatively small when the thickness of the middle ZTA layer is increased, these differences are larger for dynamic loading. When a moderate damping is included, the results do not seem to change significantly up to half the resonant frequency, as simple calculations indicate.

Some of our findings may serve researchers in the ceramic society, which work with composite materials. One of the goals is to optimize the composition of different layers to obtain the maximum strength of the laminates.[9–11] Although the loading in the uniaxial or biaxial tests is usually static and similar to point-like, the dependence of the stresses on frequency may be qualitatively similar to the one presented in **Figure 4**. For instance, up to frequencies one order of magnitude smaller than the lowest eigenfrequency, the increment of stress can be safely ignored. For larger frequencies appropriate correction factors can be used: for instance, when the applied frequency is half the lowest eigenfrequency, in our calculations the maximum stress has roughly twice the value corresponding to static loading. The order of magnitude of resonant frequency may be estimated from the characteristic time in Equation (3).

We have also touched on some other aspects, e.g., boundary conditions, distribution of pressure and the elongation of the square into rectangle. If the boundary condition with the clamped edges is replaced by the con-
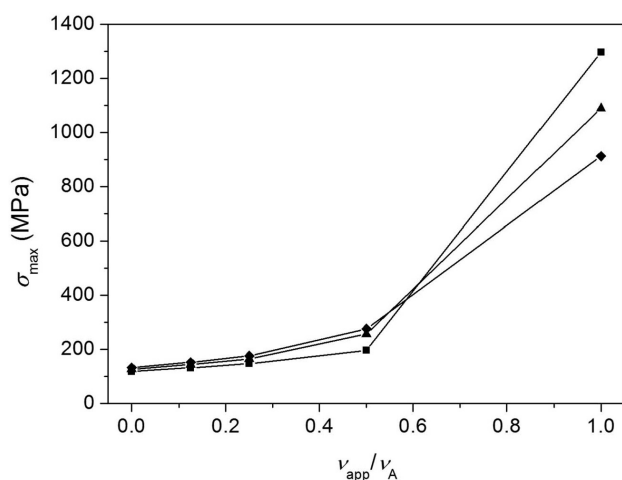


**Figure 4:** Dependence of maximum stress on the applied frequency; three samples are presented, all with thickness 5 mm: (1) pure alumina (squares); (2) composite with 4 mm ZTA inner layer and two 0.5 mm alumina outer layers (triangles); (3) composite with 4.8 mm ZTA inner layer and two 0.1 mm alumina outer layers (diamonds).

dition of freely (simply) supported edges, the deflection of $P_0$ increases as well. The increase of the deflection of $P_0$ is accompanied with the increase of the local stress. Furthermore, if the same force is locally distributed over the small area, the local stress is significantly increased. In general, we must keep in mind that the stress may not be the largest at the central point of the sample. When the square is elongated, so that the sides $2b$ in $y$–axis direction are many times larger than the sides $2a$ in $x$–axis direction, the solution for $w$ essentially depends only on $x$–coordinate in the most part of the rectangle (when the $y$–coordinate is not near the values $\pm b$). In this way we come to quasi-one-dimensional problem, which has analytical solutions for some specific problems. For instance, the static solution for $w^*$ in Equation (A.1) with constant pressure in one dimension is a polynomial of the fourth order. We have used such analytical 1D solutions as a test for the reliability of our numerical procedure.

## Acknowledgement

## 5 REFERENCES

[1] F. F. Lange, Transformation Toughening: Parts 1–5, Journal of Material Science 17 (**1982**) 5–6, 225–262

[2] M. Rühle, N. Claussen, A. H. Heuer, Transformation and Microcrack Toughening as Complementary Processes in $ZrO_2$-Toughened $Al_2O_3$, Journal of the American Ceramic Society, 69 (**1986**) 3, 195–197

[3] H. E. Lutz, N. Claussen, Duplex ceramics, Parts 1–2, Journal of the European Ceramic Society, 7 (**1991**) 209–226

[4] S. Deville, J. Chevalie, G. Fantozzi, J. F. Bartolome, J. Requena, J. S. Moya et al., Development of advanced zirconia-toughened alumina nanocomposites for orthopaedic applications, Key Engineering Materials, 264–268 (**2004**) 2012–2016

[5] N. Mandal, B. Doloi, B. Mondal, R. Das, Optimization of flank wear using Zirconia Toughened Alumina (ZTA) cutting tool: Taguchi method and Regression analysis, Measurement, 44 (**2011**) 2149–2155

[6] F. Sommer, R. Landfried, F. Kern, R. Gadov, Mechanical properties of zirconia toughened alumina with 10–24 vol. % 1Y–TZP reinforcement, Journal of the European Ceramic Society, 32 (**2012**) 4177–4184

[7] A. V. Virkar, J. F. Jue, J. J. Hansen, and R. A. Cutler, Measurement of Residual Stresses in Oxide-$ZrO_2$ Three-Layer Composites, Journal of the American Ceramic Society, 71 (**1988**) 3, C-148–151

[8] D. J. Green, P. Z. Cai, and G. L. Messing, Residual Stresses in Alumina–Zirconia Laminates, Journal of the European Ceramic Society, 19 (**1999**) 2511–2517

[9] C. H. Hsueh, Modeling of Elastic Deformation of Multilayers due to Residual Stresses and External Bending, Journal of Applied Physics, 91 (**2002**) 12, 9652–9656

[10] D. D. Barnett-Ritcey, and P. S. Nicholson, Failure Prediction Maps for a Model $Al_2O_3$ | c-$ZrO_2$/$Al_2O_3$ | $Al_2O_3$ Brittle Polycrystalline Trilayer Composite, Journal of the American Ceramic Society, 86 (**2003**) 1, 121–128

[11] M. Ambrožič, T. Kosmač, Optimization of the Bend Strength of Flat-Layered Alumina–Zirconia Composites, Journal of the American Ceramic Society, 90 (**2007**) 5, 1545–1550

[12] R. Bermejo, J. Pascual, T. Lube, R. Danzer, Optimal strength and toughness of $Al_2O_3$–$ZrO_2$ laminates designed with external or internal compressive layers, Journal of the European Ceramic Society, 28 (**2008**) 1575–1583

[13] E. Carrera, A. Ciuffreda, Bending of composites and sandwich plates subjected to localized lateral loadings: a comparison of various theories, Composite Structures, 68 (**2005**) 185–202

[14] K. F. Graff, Wave Motion in Elastic Solids (**2012**), Courier Corporation

[15] P. Lee, N. Chang, Harmonic in Elastic Sandwich Plates, Journal of Elasticity 9 (**1979**) 51–69

[16] J. Kaplunov, D. A. Prikazchikov, L. A. Prikazchikova, Dispersion of Elastic Waves in a Strongly Inhomogeneous Three-Layered Plate, International Journal of Solids and Structures 113–114 (**2017**) 169–179, doi:10.1016/j.ijsolstr.2017.01.042

[17] Z. J. Ai, C. J. Xu, G. P. Ren, Vibration of a pre-stressed plate on a transversely isotropic multilayered half-plane due to a moving load, Applied Mathematical Modeling, 59 (**2018**) 728–738, doi:10.1016/j.apm.2018.02.027

[18] M. Shariyat, M. Roshanfar, A new analytical solution and novel energy formulations for non-linear eccentric impact analysis of composite multi-layer/sandwich plates resting on point supports, Thin-Walled Structures, 127 (**2018**) 157–168, doi:10.1016/j.tws.2018.02.001

[19] S. Zhang, J. Yin, H. W. Zhang, B. S. Chen, A two-level method for static and dynamic analysis of multilayered composite beam and plate, Finite Elements in Analysis and Design, 111 (**2016**) 1–18, doi:10.1016/j.finel.2015.12.001

[20] T. Ye, G. Yin, Z. Su, Three-dimensional vibrational analysis of sandwich and multilayered plates with general ply stacking sequences by a spectral sampling surface method, Composite Structures, 176 (**2017**) 1124–1142, doi:10.1016/j.compstruct.2017.06.008

[21] W. Lacarbonara, M. Pasquali, A geometrically exact formulation for thin multi-layered laminated composite plates: Theory and experiment, Composite Structures, 93 (**2011**) 1649–1663, doi:10.1016/j.compstruct.2010.12.005

[22] L. V. Tran, S.-E. Kim, Static and free vibration analysis of multilayered plates by a higher-order shear and normal deformation theory and isogeometric analysis, Thin-Walled Structures, 130 (**2018**) 622–640, doi:10.1016/j.tws.2018.06.013

[23] Y. Wang, Z. Li, W. Chen, C. Zhang, J. Zhu, Free vibration and active control of pre-streched multilayered electroactive plates, International Journal of Solids and Structures, 180–181 (**2019**) 108–124, doi:10.1016/j.ijsolstr.2019.07.010

[24] P. Zhang, C. Qi, H. Fang, C. Ma, Y. Huang, Semi-analytical analysis of static and dynamic responses for laminated magneto-electro-elastic plates, Composite Structures, 222 (**2019**) 110933, doi:10.1016/j.compstruct.2019.110933

[25] B. Erbaş, J. Kaplunov, E. Nolde, M. Palsü, Composite wave models for elastic plates, Preceedings of Royal Society A, 474 (**2018**) 20180103, doi:10.1098/j.rspa.2018.0103

[26] L. D. Landau, E. M. Lifshitz, Theory of Elasticity, Course of Theoretical Physics, Vol. 7, Butterworth–Heinemann (**1986**)

[27] V. V. Vasiliev, Modern Conceptions of Plate Theory, Composite Structures, 48 (**2000**), 93–84.

[28] N. I. Robinson, Augmented Lévi–Michell equations for flexural plates, International Journal of Solids and Structures, 191–192 (**2020**) 497–508, doi:10.1016/j.ijsolstr.2019.12.021

**APPENDIX A:** *Dimensionless form of dynamic equation*

Using the dimensionless quantities Equation (1) transforms into:

$$D^*(\nabla^{*2})^2 w^* + \rho^* \frac{\partial^2 w^*}{\partial t^{*2}} = \frac{1}{\eta^4} p^* \qquad \text{(A.1)}$$

The Laplacian $\nabla^{*2}$ contains derivatives with respect to renormalized coordinates $x^*$ and $y^*$.

Let's take the symmetric composite with $N$ layers ($N$ is odd), denoted from "bottom" to "top" by indices $i$ from 1 to $N$. Their parameters are $h_i^* = h_i/h$, $E_i^* = E_i/E_0$, $\rho_i^* = \rho_i/\rho_0$ and $\nu_i$. The total thickness $h$ is the sum of thicknesses $h_i$ of all layers. The dimensionless flexural rigidity is:

$$D^* = \frac{1}{3} \sum_{i=1}^N \frac{E_i^*}{1-\nu_i^2}\left[(z_{iT}^*)^3 - (z_{iB}^*)^3\right] \qquad \text{(A.2)}$$

Their symbols $z_{iT}^*$ and $z_{iB}^*$ mean the dimensionless $z$–coordinates of the top and the bottom side of the $i$–th layer, respectively. The neutral plane is at $z^* = 0$ due to symmetry. We have derived Equation (A.2) in a similar manner as the derivation of flexural rigidity for homogeneous plate in the textbook of Landau and Lifshitz.[26] The case with $N = 1$ (homogeneous plate) gives the expression according to Equation (2) in physical units. The effective density is:

$$\rho^* = \sum_{i=1}^N \rho_i^* h_i^* \qquad \text{(A.3)}$$

The 2D stress tensor in $i$-th layer is:

$$\sigma = -\frac{E_i}{1-\nu_i^2} \eta^2 z^* \cdot \begin{bmatrix} \dfrac{\partial^2 w^*}{\partial x^{*2}} + \nu_i \dfrac{\partial^2 w^*}{\partial y^{*2}} & (1-\nu_i)\dfrac{\partial^2 w^*}{\partial x^* \partial y^*} \\[3mm] (1-\nu_i)\dfrac{\partial^2 w^*}{\partial x^* \partial y^*} & \dfrac{\partial^2 w^*}{\partial y^{*2}} + \nu_i \dfrac{\partial^2 w^*}{\partial x^{*2}} \end{bmatrix}$$

$$\text{(A.4)}$$

We give a few notes about the numerical procedure that we have developed. A discrete quadratic network of equidistant points, typically with size 201×201, was used. Fourth-order spatial derivatives of $w^*$, appearing in the double-Laplacian term, were derived on the basis of finite differences for neighboring points, in analogy to elliptic equations. As regards the time relaxation procedure, the problem of the second order in time derivative was transformed into the problem of first order by tracing variables $w$ and the derivative $\partial w/\partial t$ at all discrete points in network. This enabled us to use a kind of Runge-Kutta method of second order, but simultaneously for all points in network. The numerical reliability for an appropriately chosen small time step was checked by halving the time step and comparing the results.